Received: 5 July 2019 | Revised: 7 January 2020 | Accepted: 12 January 2020

DOI: 10.1111/cas.14327

ORIGINAL ARTICLE

Cancer Science WILEY

Replisome genes regulation by antitumor *miR-101-5p* in clear cell renal cell carcinoma

Yasutaka Yamada[1,2] | Nijiro Nohata[3] | Akifumi Uchida[4] | Mayuko Kato[1,2] | Takayuki Arai[1,2] | Shogo Moriya[5] | Keiko Mizuno[4] | Satoko Kojima[6] | Kazuto Yamazaki[7] | Yukio Naya[6] | Tomohiko Ichikawa[2] | Naohiko Seki[1]

[1]Department of Functional Genomics, Chiba University Graduate School of Medicine, Chiba, Japan

[2]Department of Urology, Chiba University Graduate School of Medicine, Chiba, Japan

[3]MSD K.K., Tokyo, Japan

[4]Department of Pulmonary Medicine, Kagoshima University Graduate School of Medical and Dental Sciences, Kagoshima, Japan

[5]Department of Biochemistry and Genetics, Chiba University Graduate School of Medicine, Chiba, Japan

[6]Department of Urology, Teikyo University Chiba Medical Center, Ichihara, Japan

[7]Department of Pathology, Teikyo University Chiba Medical Center, Ichihara, Japan

Correspondence
Naohiko Seki, Department of Functional Genomics, Chiba University Graduate School of Medicine, 1-8-1 Inohana Chuo-ku, Chiba 260-8670, Japan.
Email: naoseki@faculty.chiba-u.jp

Funding information
KAKENHI grant, Grant/Award Number: 16H05462, 17K11160, 18K09338, 18K16685, 18K16723 and 18K16724

Abstract

Analysis of microRNA (miRNA) regulatory networks is useful for exploring novel biomarkers and therapeutic targets in cancer cells. The Cancer Genome Atlas dataset shows that low expression of both strands of pre-*miR-101* (*miR-101-5p* and *miR-101-3p*) significantly predicted poor prognosis in clear cell renal cell carcinoma (ccRCC). The functional significance of *miR-101-5p* in cancer cells is poorly understood. Here, we focused on *miR-101-5p* to investigate the antitumor function and its regulatory networks in ccRCC cells. Ectopic expression of mature miRNAs or siRNAs was investigated in cancer cell lines to characterize cell function, ie, proliferation, apoptosis, migration, and invasion. Genome-wide gene expression and in silico database analyses were undertaken to predict miRNA regulatory networks. Expression of *miR-101-5p* caused cell cycle arrest and apoptosis in ccRCC cells. Downstream neighbor of son (*DONSON*) was directly regulated by *miR-101-5p*, and its aberrant expression was significantly associated with shorter survival in propensity score-matched analysis ($P = .0001$). Knockdown of *DONSON* attenuated ccRCC cell aggressiveness. Several replisome genes controlled by *DONSON* and their expression were closely associated with ccRCC pathogenesis. The antitumor *miR-101-5p*/*DONSON* axis and its modulated replisome genes might be a novel diagnostic and therapeutic target for ccRCC.

KEYWORDS

DONSON, microRNA, *miR-101-5p*, renal cell carcinoma, replisome

1 | INTRODUCTION

Renal cell carcinoma (RCC) accounts for approximately 3% of adult malignancies and is the 12th most prevalent malignancy worldwide, with 338 000 newly diagnosed patients in 2012 and approximately 100 000 deaths annually.[1] Clear cell RCC (ccRCC) is pathologically the most common type and accounts for approximately 75% of all cases.[2] Although the prognosis is favorable with surgical resection for nonmetastatic RCC, approximately 20%-30% of RCC patients have metastatic sites at the diagnosis and the 5-year survival rate is less than 20%.[2,3] In addition, more than 20% of patients develop metastases during postoperative follow-up periods.[4] These clinical issues are caused by a lack of useful biomarkers for early detection of RCC and the inefficiency of therapy for patients with metastatic or treatment-resistant RCC.

MicroRNAs (miRNAs) are classified as noncoding RNAs that are approximately 18-25 bases in size. They are widely found, ranging from plants to humans.[5] MicroRNAs bind to the 3′-UTR of target genes and have many biological functions that are achieved by regulating the expression of protein-coding genes in a sequence-dependent manner.[6] Numerous reports have indicated that miRNAs are closely involved in cell growth, migration, invasion, apoptosis, angiogenesis, and tumor metastasis in various human cancers.[7] Interestingly, a single miRNA can regulate a vast number of protein-coding or noncoding RNAs. Therefore, the analysis of aberrantly expressed miRNAs in human cancers provides us information about cancer-modulating molecular networks.

Previously, we established a miRNA expression signature from autopsy samples of ccRCC patients who relapsed following sunitinib treatment.[8] Based on this signature, we have identified a number of antitumor microRNAs (*miR-101-3p*, *miR-455*-duplex, and the *miR-29*-family) as well as the oncogenes that they control. All of the miRNAs were closely related to ccRCC development.[8-10] The discovery of oncogenic networks mediated by antitumor miRNAs contributes to the elucidation of the molecular mechanisms mediating the pathogenesis of ccRCC.

Current RNA-sequencing (-seq) technology makes it possible to construct miRNA expression signatures in human cancer. Expressions of several passenger strands of miRNA are significantly up- or down-regulated in cancer tissues from the miRNA signature.[11,12] Our functional assays showed that several passenger strands of miRNAs (eg, *miR-455-5p*, *miR-144-5p*, and *miR-145-3p*) had antitumor roles, as did the guide strands of miRNAs.[9,11,13-15] In general, the passenger strand of miRNA is degraded and therefore considered to have no function.[16] Our reports differ from the previous concept. Thus, we have discovered a new aspect of miRNA functionality.

Here, we focused on *miR-101-5p* (the passenger strand) to elucidate the function of *miR-101-5p* and determine its target oncogenes as useful diagnostic markers in ccRCC. Previous studies have shown that *miR-101-3p* (the guide strand of the *miR-101* duplex) acts as an antitumor miRNA in several cancers by targeting oncogenic genes.[8,17] In contrast to *miR-101-3p*, the functional significance of *miR-101-5p* in cancer cells is poorly understood. Ectopic expression of *miR-101-5p* attenuated the aggressive phenotype of ccRCC cells. Downstream neighbor of son (*DONSON*) was directly regulated by *miR-101-5p*, and its aberrant expression was significantly associated with shorter survival in propensity score-matched analysis. Moreover, several replisome genes controlled by *DONSON* and their expression were closely associated with ccRCC pathogenesis.

2 | MATERIALS AND METHODS

2.1 | Clinical samples and cell lines

In the present study, 18 clinical ccRCC tissue samples were obtained from patients received nephrectomy at Chiba University Hospital between 2014 and 2015 (Table S1). Also, autopsy specimens were obtained from 5 patients whose disease was resistant to several tyrosine kinase inhibitor (TKI) treatments; samples were obtained from Teikyo University Chiba Medical Center Hospital between 2012 and 2016 (Table S2). We obtained informed consent from all patients and the current research protocol was approved by the Institutional Review Board of Chiba University (acceptance no. 484). Two ccRCC cell lines (786-0 and A498) from ATCC were used in this study. These cell lines were cultured in RPMI-1640 with 10% FBS (HyClone).

2.2 | Transfection of ccRCC cells with miRNAs, siRNAs, and plasmid vectors

MicroRNAs, siRNAs, and vectors were transfected into cancer cells as described in our previous reports using the reagents listed in Table S3.[18]

2.3 | RNA preparation and quantitative RT-PCR

Total RNA including miRNA was isolated using TRIzol reagent (Invitrogen) in clinical specimens and ISOGEN reagent (Nippon Gene) in ccRCC cells.

TaqMan probes and *DONSON* primers were used and the reagents are listed in Table S3. Quantitative RT-PCR for *miR-101-5p* and *miR-101-3p* was used to validate miRNA expression. To normalize the data for analysis of mRNAs and miRNAs, *GUSB* and *RNU48* were used. The PCR quantification was carried out as previously described.[19,20]

2.4 | Assays of proliferation, migration, and invasion

Cell proliferation, migration, and invasion were assessed as described previously.[19,20]

2.5 | Assay of cell cycle

Clear cell RCC cells were transfected with either the transfection reagents alone as a control or *miR-101-5p*, *miR-101-3p*, and si-*DONSON* in 6-well tissue culture plates. Seventy-two hours after transfection, these cells were harvested by trypsinization. Cells were stained with propidium iodide with the Cycletest Plus DNA Reagent Kit (BD Biosciences) and analyzed using the CyAn ADP analyzer (BD Biosciences). The proportion of cells in the G_0/G_1, S and G_2/M phases were calculated and compared. We undertook each experiment in triplicate.

2.6 | Assay of apoptosis

In order to identify the apoptotic cells, the FITC Annexin V apoptosis detection kit (BD Biosciences) and the BD FACS Celesta flow cytometer (BD Biosciences) were used according to the

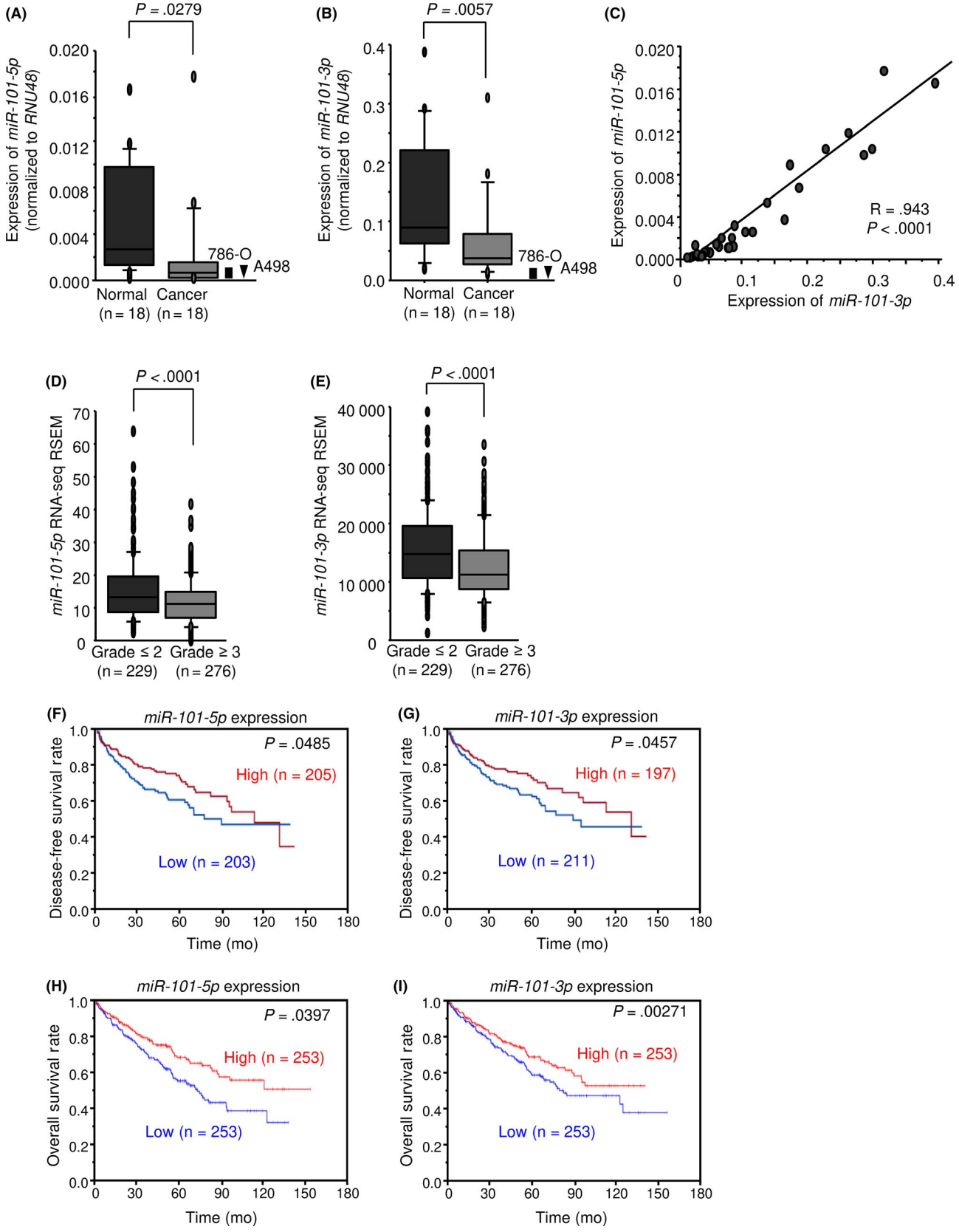

FIGURE 1 Expression of *miR-101* and its clinical significance in clear cell renal cell carcinoma (ccRCC). A-C, Expression levels of *miR-101-5p* and *miR-101-3p* in ccRCC clinical specimens. *RNU48* was used as an internal control. Expression levels of *miR-101-5p* and *miR-101-3p* were positively correlated by Spearman's rank test. D, E, Based on The Cancer Genome Atlas database, high grades of RCC were significantly associated with low *miR-101* expression levels. F-I, Low expression levels of *miR-101* were significantly associated with poor prognosis in RCC patients (disease-free survival and overall survival). RNA-seq, RNA sequencing; RSEM, RNA sequencing by expectation-maximization

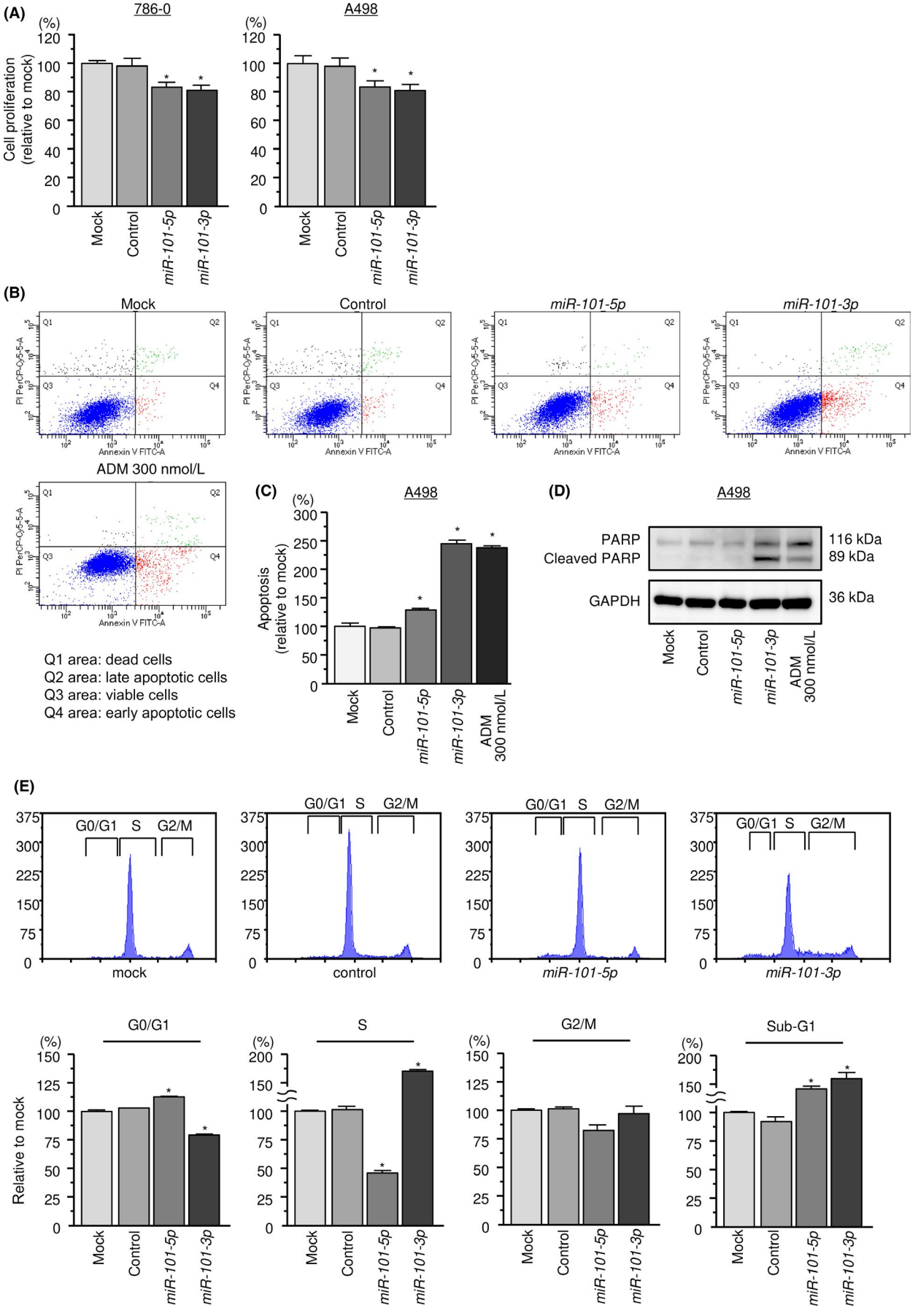
(A)
786-0
A498
(%)
Cell proliferation (relative to mock)
Mock
Control
miR-101-5p
miR-101-3p
(B)
Mock
Control
miR-101-5p
miR-101-3p
ADM 300 nmol/L
PI PerCP-Cy5-5-A
Annexin V FITC-A
Q1 area: dead cells
Q2 area: late apoptotic cells
Q3 area: viable cells
Q4 area: early apoptotic cells
(C)
A498
Apoptosis (relative to mock)
ADM 300 nmol/L
(D)
A498
PARP
Cleaved PARP
GAPDH
116 kDa
89 kDa
36 kDa
(E)
G0/G1
S
G2/M
mock
control
miR-101-5p
miR-101-3p
Relative to mock
Sub-G1

FIGURE 2 Functional analysis of *miR-101*-duplex in clear cell renal cell carcinoma cells. A, Cell proliferation after introduction of the *miR-101*-duplex. B-D, Effect of *miR-101* on apoptosis, as assessed by apoptosis assays and western blot analysis of cleaved poly (ADP-ribose) polymerase (PARP), as a marker of apoptosis. *GAPDH* was used as the loading control. Adriamycin (ADM) was used as a positive control. E, Effect of *miR-101* on the cell cycle. Flow cytometric analyses of cell-cycle-phase distribution in control cells and cells transfected with the *miR-101*. Bar charts represent the percentages of inhibitor-transfected cells relative to the control cells in the G_0/G_1, S, G_2/M, and sub-G_1 phases, respectively. $^*P < .0001$

manufacturer's instructions. We classified these cells as viable cells, dead cells, or early or late apoptotic cells and compared the percentage of apoptotic cells according to each condition. To evaluate apoptosis with western blotting, anti-poly (ADP-ribose) polymerase (PARP) was used. Adriamycin (ADM) was used as a positive control.

2.7 | Incorporation of miR-101-5p and miR-101-3p into the RNA-induced silencing complex by Ago2 immunoprecipitation

After 72 hours, miRNAs incorporated into the RNA-induced silencing complex (RISC) were isolated a human AGO2 miRNA isolation kit (Wako Pure Chemical Industries). The method of measuring the amount of *miR-101-5p* incorporated into RISC was according to a previous study.[14]

2.8 | Target genes regulated by miR-101-5p and miR-101-3p

Candidate target genes regulated by *miR-101-5p* or *miR-101-3p* were identified using in silico and genome-wide gene expression analyses and those obtained from the TargetScan database (http://www.targetscan.org/vert_70/). Upregulated genes in RCC tissues compared with normal renal tissues were identified from public data in the Gene Expression Omnibus (GEO; accession no. GSE36895), from which we narrowed down these genes. Gene expression was analyzed with our oligo microarray data analyses (Human GE 60K; Agilent Technologies) that were deposited into the GEO (on 23 August 2018; http://www.ncbi.nlm.nih.gov/geo/) with accession number GSE118966.

2.9 | Evaluation of miR-101-5p binding sites by luciferase reporter assay

The 3′-UTR of *DONSON* and the 3′-UTR lacking the putative *miR-101-5p* binding site (position 219-225 in 3′-UTR of *DONSON*) were cloned into the psiCHECk-2 vector. A luciferase reporter assay was undertaken as previously described.[19,20]

2.10 | Western blot analysis and immunohistochemistry

Western blotting and immunohistochemistry (IHC) were carried out as described previously.[19,20] Primary Abs are listed in Table S3. Tissue microarray (KD485S; Cosmo Bio) was used to show *DONSON* expression in normal kidney tissue with IHC.

2.11 | Downstream genes of *DONSON*

To elucidate *DONSON*-regulated pathways in ccRCC cells, we analyzed gene expression fluctuation in 786-O cells transfected with si-*DONSON*. Microarray data were used for expression signatures of si-*DONSON* transfectants. The data were registered to the GEO on 4 December 2018 (accession no. GSE123317).

2.12 | Clinical significance of miR-101 and DONSON

We examined the clinical importance of miRNAs and genes in RCC patients using the RNA-seq database in The Cancer Genome Atlas (TCGA; https://tcga-data.nci.nih.gov/tcga/). Expression data and clinical information of these molecules were acquired from cBioPortal (http://www.cbioportal.org/) and the provisional data were downloaded on 8 January 2019.[21-23] We calculated the *Z* scores as the mRNA expression values. Gene Set Enrichment Analysis (GSEA) was undertaken based on mRNA-seq data from cBioPortal. A heatmap of gene expression was provided by the RCC-RNA-seq database.

2.13 | Statistical analyses

The Mann-Whitney *U* test was applied to compare between 2 groups. For multiple groups, one-way ANOVA and Tukey tests for post-hoc analyses was applied. These analyses were carried out with GraphPad Prism7 (GraphPad Software) and JMP Pro 14 (SAS Institute). Expert StatView (version 5; SAS Institute) was used for other analyses.

3 | RESULTS

3.1 | Analysis of miR-101-5p and miR-101-3p expression levels in clinical ccRCC tissues and their clinical significance

In the human genome, the chromosomal location of *miR-101* is at 1q31.3. The mature sequences of *miR-101-5p* and *miR-101-3p* are 5′-CAGUUAUCACAGUGCUGAUGCU-3′ and 5′-UACAGUACUGUGAUAACUGAA-3′, respectively. Both *miR-101-5p* and *miR-101-3p* expressions were significantly reduced in ccRCC tissues compared

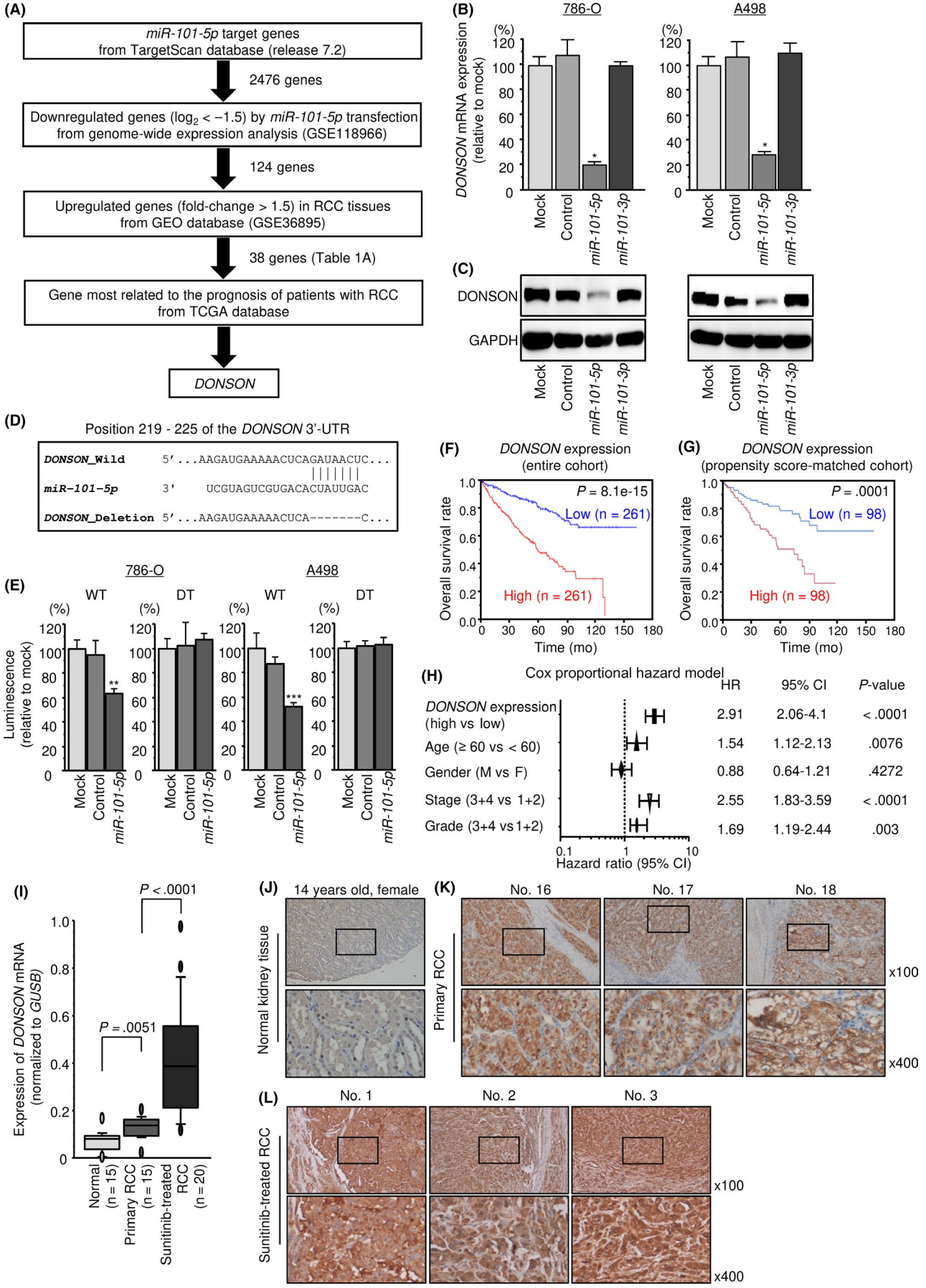
(A)
miR-101-5p target genes from TargetScan database (release 7.2)
2476 genes
Downregulated genes (log2 < −1.5) by miR-101-5p transfection from genome-wide expression analysis (GSE118966)
124 genes
Upregulated genes (fold-change > 1.5) in RCC tissues from GEO database (GSE36895)
38 genes (Table 1A)
Gene most related to the prognosis of patients with RCC from TCGA database
DONSON
(B)
786-O
A498
DONSON mRNA expression (relative to mock)
Mock
Control
miR-101-5p
miR-101-3p
(C)
DONSON
GAPDH
(D)
Position 219 - 225 of the DONSON 3'-UTR
DONSON_Wild 5'...AAGAUGAAAAACUCAGAUAACUC...
miR-101-5p 3' UCGUAGUCGUGACACUAUUGAC
DONSON_Deletion 5'...AAGAUGAAAAACUCA-------C...
(E)
786-O
A498
WT
DT
Luminescence (relative to mock)
(F)
DONSON expression (entire cohort)
P = 8.1e-15
Low (n = 261)
High (n = 261)
Overall survival rate
Time (mo)
(G)
DONSON expression (propensity score-matched cohort)
P = .0001
Low (n = 98)
High (n = 98)
(H)
Cox proportional hazard model
HR
95% CI
P-value
DONSON expression (high vs low) 2.91 2.06-4.1 < .0001
Age (≥ 60 vs < 60) 1.54 1.12-2.13 .0076
Gender (M vs F) 0.88 0.64-1.21 .4272
Stage (3+4 vs 1+2) 2.55 1.83-3.59 < .0001
Grade (3+4 vs 1+2) 1.69 1.19-2.44 .003
Hazard ratio (95% CI)
(I)
P < .0001
P = .0051
Expression of DONSON mRNA (normalized to GUSB)
Normal (n = 15)
Primary RCC (n = 15)
Sunitinib-treated RCC (n = 20)
(J)
14 years old, female
Normal kidney tissue
Primary RCC
(K)
No. 16
No. 17
No. 18
x100
x400
(L)
No. 1
No. 2
No. 3
Sunitinib-treated RCC
x100
x400

FIGURE 3 *miR-101-5p* candidate target gene and its clinical significance. A, Strategy for searching for oncogenes targeted by *miR-101-5p* in clear cell renal cell carcinoma (ccRCC). B, *DONSON* mRNA expression levels 48 h after transfection of ccRCC cells with 10 nM *miR-101-5p* or *miR-101-3p*. *GAPDH* was used as an internal control. C, Protein expression of DONSON 72 h after transfection with *miR-101-5p* or *miR-101-3p*. GAPDH was used as a loading control. D, E, Dual luciferase reporter assays with vectors encoding the putative *miR-101-5p* target site in the WT *DONSON* 3′-UTR and a 3′-UTR with the target sites deleted (deletion-type (DT)). Normalized data were calculated as the ratio of *Renilla*/firefly luciferase activities. F, G, Kaplan-Meier analyses for overall survival in the entire cohort and propensity score-matched cohort. Patients were divided into 2 groups according to *DONSON* expression levels: high expression (red line) and low expression (blue line). H, Multivariate analysis of overall survival with clinical parameters, including *DONSON* expression. I, *DONSON* mRNA expression levels in normal, primary (sunitinib-naïve) ccRCC and sunitinib-treated ccRCC patients. J-L, Immunostaining showed the expression of DONSON in normal kidney tissue, primary ccRCC, and sunitinib-treated ccRCC (100× and 400× magnification fields). *P < .0001; **P < .005; ***P < .01. CI, confidence interval; GEO, Gene Expression Omnibus; TCGA, The Cancer Genome Atlas

with those in adjacent noncancerous tissues (P = .027 and P = .0057, respectively; Figure 1A,B). In addition, Spearman's rank analysis showed strong positive correlation between *miR-101-5p* and *miR-101-3p* expression levels (R = 0.943, P < .0001; Figure 1C). From a large cohort of TCGA database, low expressions of *miR-101-5p* and *miR-101-3p* were significantly associated with high pathological grade (both, P < .0001; Figure 1D,E) and poor clinical outcomes (disease-free survival, P = .0485 and P = .0457; overall survival, P = .0397 and P = .00271, respectively, Figure 1F-I) in ccRCC patients.

3.2 | Antitumor functions of miR-101-5p and miR-101-3p in ccRCC cells

Restoration of *miR-101-5p* and *miR-101-3p* expression indicated that both miRNAs significantly suppressed cancer cell proliferation (Figure 2A), migration (Figure S1A,B) and invasion potentials (Figure S1C,D).

Furthermore, the apoptotic rate was elevated in *miR-101-5p* and *miR-101-3p* transfected cells compared to controls (Figure 2B,C). In addition, transfection of *miR-101-3p* apparently upregulated cleaved PARP expression (Figure 2D). In cell cycle analyses, ectopic expression of these miRNAs confirmed increase in the sub-G_1 peak in ccRCC cells (Figure 2E). We analyzed the expression levels of cell cycle-related genes by ectopic expression of *miR-101-5p* and/or *miR-101-3p* in ccRCC cells (Table S4). Downregulation of *CCNB1*, *CDK1*, *CDK2*, and *CDK4* were detected by microarray data.

Cell migration and invasive abilities were significantly inhibited by ectopic expression of *miR-101-5p* and *miR-101-3p* in ccRCC cells. To explain this phenomenon, the expression of epithelial-mesenchymal transition (EMT)-related genes was examined by microarray analyses (Table S4). The mRNA expression levels of *CDH2*, *VIM*, *ZEB1*, *TWIST1*, *SNAI1*, and *FN1* were reduced by *miR-101-5p* and/or *miR-101-3p* transfection into ccRCC cells. Furthermore, we investigated the expression changes of EMT-related proteins (eg, E-cadherin, N-cadherin, SLUG, Vimentin, and TWIST) by ectopic expression of *miR-101-5p* and *miR-101-3p* in ccRCC cells (Figure S2). Notably, the expression levels of N-cadherin, SLUG, and Vimentin were suppressed by expressions of *miR-101-5p* and *miR-101-3p* in 2 RCC cell lines, 786-O and A498 (Figure S2). Downregulation of TWIST was detected in 786-O cells by *miR-101-5p* expression. Our present data indicated that expression of these miRNAs regulate the expression of EMT-related proteins and they play critical roles in malignant transformation of ccRCC cells.

In addition, we examined the synergistic effect of the 2 miRNAs on cell proliferation, apoptosis, and the cell cycle. No synergistic effect of antitumor effects in RCC cells by the ectopic expression of the 2 miRNAs, *miR-101-5p* and *miR-101-3p*, was observed (Figure S3).

3.3 | Incorporation of miR-101-5p into RISC in ccRCC cells

To verify that *miR-101-5p* (passenger strand) had actual functions in ccRCC cells, it is essential that miRNAs are incorporated into the RISC to control target genes. Immunoprecipitation using anti-Ago2 Abs was carried out after transfection of *miR-101-5p* into 786-O cells. The amount of *miR-101-5p* incorporated into the protein was measured by PCR. Levels of *miR-101-5p* in the immunoprecipitation were much higher than those in mock, miR-control, or *miR-101-3p*-transfected cells (P < .0001; Figure S4).

3.4 | Candidate target genes of miR-101-5p and miR-101-3p

We identified genes that had putative target sites for *miR-101* in their 3′-UTR and that showed downregulated expression in ccRCC cells transfected with *miR-101* ($\log_2$ ratio less than −1.5) and upregulated expression levels (fold-change greater than 1.5) in RCC tissues from the GEO database (Figure 3A). Using this search strategy, 38 and 47 genes were found as candidate target genes for *miR-101-5p* and *miR-101-3p*, respectively (Table 1). Among these genes, we focused on *DONSON*, which is targeted by *miR-101-5p* and had the strongest relation to the prognosis from TCGA database.

3.5 | MicroRNA-101-5p targeted *DONSON* expression

mRNA and protein levels of DONSON were significantly reduced after transfection of 786-0 and A498 cells with *miR-101-5p* compared to control cells (Figure 3B,C).

TABLE 1 *miR-101*-duplex regulatory genes in clear cell renal cell carcinoma cells

Gene symbol	Gene name	Entrez Gene ID	Cytoband	GEO expression fold-change (tumor/normal)	Mock vs miR-101-5p transfection in 786-O cells (log2 ratio)	OS analysis from TCGA database (high vs low expression, *P* value)
(A) *miR-101-5p*						
DONSON	Downstream neighbor of SON	29980	hs|21q22.11	1.665	−1.952	8.10E-15
EFHD2	EF-hand domain family, member D2	79180	hs|1p36.21	2.000	−1.933	1.16E-05
NAP1L1	Nucleosome assembly protein 1-like 1	4673	hs|12q21.2	1.536	−1.672	1.40E-05
HSPA6	Heat shock 70 kDa protein 6 (HSP70B')	3310	hs|1q23.3	2.814	−1.509	0.000116
PBK	PDZ binding kinase	55872	hs|8p21.1	2.982	−2.425	0.0018800
DPYSL3	Dihydropyrimidinase-like 3	1809	hs|5q32	2.327	−1.548	0.0038900
EVI2A	Ecotropic viral integration site 2A	2123	hs|17q11.2	2.971	−1.682	0.0073700
KIAA1841	KIAA1841	84542	hs|2p15	2.132	−1.658	0.0106000
SNX10	Sorting nexin 10	29887	hs|7p15.2	1.564	−2.843	0.0112000
GINS1	GINS complex subunit 1 (Psf1 homolog)	9837	hs|20p11.21	1.532	−2.077	0.0137000
LYSMD2	LysM, putative peptidoglycan-binding, domain containing 2	256586	hs|15q21.2	1.433	−1.687	0.0244000
TBL1XR1	Transducin (beta)-like 1 X-linked receptor 1	79718	hs|3q26.32	1.427	−1.879	0.0396000
KCND2	Potassium voltage-gated channel, Shal-related subfamily, member 2	3751	hs|7q31.31	2.588	−1.551	0.0444000
ITGA5	Integrin, alpha 5 (fibronectin receptor, alpha polypeptide)	3678	hs|12q13.13	7.156	−1.932	0.0818000
MEGF6	Multiple EGF-like-domains 6	1953	hs|1p36.32	2.113	−1.608	0.1510000
KDELC2	KDEL (Lys-Asp-Glu-Leu) containing 2	143888	hs|11q22.3	1.710	−1.651	0.1690000
CD109	CD109 molecule	135228	hs|6q13	1.449	−1.739	0.2230000
MET	Met proto-oncogene	4233	hs|7q31.2	2.553	−2.159	0.2240000
HAUS6	HAUS augmin-like complex, subunit 6	54801	hs|9p22.1	1.831	−2.069	0.2980000
FCHSD2	FCH and double SH3 domains 2	9873	hs|11q13.4	1.482	−1.645	0.3190000
QSER1	Glutamine and serine rich 1	79832	hs|11p13	1.565	−2.025	0.3800000
NCAPG2	Non-SMC condensin II complex, subunit G2	54892	hs|7q36.3	2.127	−2.679	0.3850000
MEF2C	Myocyte enhancer factor 2C	4208	hs|5q14.3	2.693	−1.988	0.4720000
PMP22	Peripheral myelin protein 22	5376	hs|17p12	3.152	−1.938	0.4800000
METAP1D	Methionyl aminopeptidase type 1D (mitochondrial)	254042	hs|2q31.1	1.492	−1.645	0.4810000
IL16	Interleukin 16	3603	hs|15q25.1	1.799	−1.642	0.6600000
EGLN3	Egl-9 family hypoxia-inducible factor 3	112399	hs|14q13.1	13.669	−1.568	0.6880000
CKAP2	Cytoskeleton associated protein 2	26586	hs|13q14.3	1.454	−1.803	0.8310000
PCSK5	Proprotein convertase subtilisin/kexin type 5	5125	hs|9q21.13	1.490	−2.535	0.0000246[a]
MXI1	MAX interactor 1, dimerization protein	4601	hs|10q25.2	1.987	−2.013	0.0000979[a]
KCTD20	Potassium channel tetramerization domain containing 20	222658	hs|6p21.31	1.415	−1.582	0.0006140[a]
LRRC8C	Leucine rich repeat containing 8 family, member C	84230	hs|1p22.2	1.890	−1.593	0.0039200[a]
RCBTB2	Regulator of chromosome condensation (RCC1) and BTB (POZ) domain containing protein 2	1102	hs|13q14.2	1.456	−2.255	0.0054900[a]
EDIL3	EGF-like repeats and discoidin I-like domains 3	10085	hs|5q14.3	2.902	−2.611	0.0085400[a]

(Continues)

TABLE 1 (Continued)

Gene symbol	Gene name	Entrez Gene ID	Cytoband	GEO expression fold-change (tumor/normal)	Mock vs miR-101-5p transfection in 786-O cells (log2 ratio)	OS analysis from TCGA database (high vs low expression, *P* value)
TPR	Translocated promoter region, nuclear basket protein	7175	hs|1q31.1	1.663	−1.630	0.0124000[a]
NR3C1	Nuclear receptor subfamily 3, group C, member 1 (glucocorticoid receptor)	2908	hs|5q31.3	2.111	−1.718	0.0178000[a]
STARD13	StAR-related lipid transfer (START) domain containing 13	90627	hs|13q13.1	1.445	−2.355	0.0374000[a]
SETD7	SET domain containing (lysine methyltransferase) 7	80854	hs|4q31.1	2.225	−2.392	0.0459000[a]

Gene symbol	Gene name	Entrez Gene ID	Cytoband	GEO expression fold-change (tumor/normal)	Mock vs miR-101-3p transfection in 786-O cells (log2 ratio)	OS analysis from TCGA database (high vs low expression, *P* value)
(B) *miR-101-3p*						
JAK3	Janus kinase 3	3718	hs|19p13.11	2.283	−1.516	1.23E-09
MX2	Myxovirus (influenza virus) resistance 2 (mouse)	4600	hs|21q22.3	1.508	−1.830	3.81E-08
NAP1L1	Nucleosome assembly protein 1-like 1	4673	hs|12q21.2	1.536	−1.795	1.40E-05
TMEM39B	Transmembrane protein 39B	55116	hs|1p35.1	2.416	−1.037	2.64E-05
ANXA2	Annexin A2	302	hs|15q22.2	1.659	−1.811	0.000151
STIL	SCL/TAL1 interrupting locus	6491	hs|1p33	2.136	−1.176	0.000255
FBXO32	F-box protein 32	114907	hs|8q24.13	1.485	−1.079	0.000574
LMNB1	Lamin B1	4001	hs|5q23.2	2.245	−3.395	0.002780
AP3S1	Adaptor-related protein complex 3, sigma 1 subunit	1176	hs|5q23.1	1.622	−1.320	0.022000
SELPLG	Selectin P ligand	6404	hs|12q24.11	2.757	−1.457	0.026600
RASD2	RASD family, member 2	23551	hs|22q12.3	2.707	−1.957	0.080900
NAV1	Neuron navigator 1	89796	hs|1q32.1	2.247	−1.055	0.086600
MAD2L1	MAD2 mitotic arrest deficient-like 1 (yeast)	4085	hs|4q27	1.954	−1.418	0.092900
TTYH2	Tweety family member 2	94015	hs|17q25.1	1.958	−1.103	0.097200
DDIT4	DNA-damage-inducible transcript 4	54541	hs|10q22.1	3.996	−1.103	0.148000
IKZF3	IKAROS family zinc finger 3 (Aiolos)	22806	hs|17q12	2.099	−1.098	0.165000
RRM1	Ribonucleotide reductase M1	6240	hs|11p15.4	1.836	−1.294	0.173000
NETO2	Neuropilin (NRP) and tolloid (TLL)-like 2	81831	hs|16q12.1	10.418	−1.545	0.191000
IKZF2	IKAROS family zinc finger 2 (Helios)	22807	hs|2q34	1.499	−2.151	0.221000
ZCCHC2	Zinc finger, CCHC domain containing 2	54877	hs|18q21.33	2.171	−1.391	0.247000
CEBPA	CCAAT/enhancer binding protein (C/EBP), alpha	1050	hs|19q13.11	1.531	−1.176	0.320000
ITGA3	Integrin, alpha 3 (antigen CD49C, alpha 3 subunit of VLA-3 receptor)	3675	hs|17q21.33	1.486	−1.224	0.325000
CPNE8	Copine VIII	144402	hs|12q12	1.513	−1.306	0.352000
STAT1	Signal transducer and activator of transcription 1, 91kDa	6772	hs|2q32.2	1.550	−1.047	0.376000

(Continues)

TABLE 1 (Continued)

Gene symbol	Gene name	Entrez Gene ID	Cytoband	GEO expression fold-change (tumor/normal)	Mock vs miR-101-3p transfection in 786-O cells (log2 ratio)	OS analysis from TCGA database (high vs low expression, *P* value)
STC2	Stanniocalcin 2	8614	hs|5q35.1	6.507	−1.152	0.440000
NCF2	Neutrophil cytosolic factor 2	4688	hs|1q25.3	3.432	−1.545	0.495000
ZNF532	Zinc finger protein 532	55205	hs|18q21.32	1.899	−1.237	0.504000
FAM78A	Family with sequence similarity 78, member A	286336	hs|9q34.13	4.577	−1.504	0.534000
BAZ2A	Bromodomain adjacent to zinc finger domain, 2A	11176	hs|12q13.3	1.700	−1.433	0.739000
MCTP1	Multiple C2 domains, transmembrane 1	79772	hs|5q15	3.092	−1.720	0.749000
RAB27A	RAB27A, member RAS oncogene family	5873	hs|15q21.3	1.452	−1.602	0.766000
CARD8	Caspase recruitment domain family, member 8	22900	hs|19q13.33	1.650	−1.535	0.854000
RPS6KA5	Ribosomal protein S6 kinase, 90kDa, polypeptide 5	9252	hs|14q32.11	1.480	−1.155	6.28E-06[a]
PCSK5	Proprotein convertase subtilisin/kexin type 5	5125	hs|9q21.13	1.490	−1.503	2.46E-05[a]
ZNF792	Zinc finger protein 792	126375	hs|19q13.11	1.534	−1.348	0.000156[a]
TGFA	transforming growth factor, alpha	7039	hs|2p13.3	2.497	−1.122	0.000477[a]
NRP1	Neuropilin 1	8829	hs|10p11.22	1.509	−1.199	0.001140[a]
SPRY1	Sprouty homolog 1, antagonist of FGF signaling (Drosophila)	10252	hs|4q28.1	1.622	−1.125	0.003680[a]
CDH5	Cadherin 5, type 2 (vascular endothelium)	1003	hs|16q21	2.616	−1.448	0.009350[a]
ICK	Intestinal cell (MAK-like) kinase	22858	hs|6p12.2	1.619	−1.514	0.011900[a]
CDK19	Cyclin-dependent kinase 19	23097	hs|6q21	2.174	−1.108	0.016600[a]
NAA15	N(alpha)-acetyltransferase 15, NatA auxiliary subunit	80155	hs|4q31.1	1.460	−2.003	0.020100[a]
MLEC	Malectin	9761	hs|12q24.31	1.519	−1.385	0.020400[a]
BDP1	B double prime 1, subunit of RNA polymerase III transcription initiation factor IIIB	55814	hs|5q13.2	1.448	−1.272	0.021800[a]
CBL	Cbl proto-oncogene, E3 ubiquitin protein ligase	867	hs|11q23.3	1.800	−1.027	0.051800[a]
EMP1	Epithelial membrane protein 1	2012	hs|12p13.1	1.615	−1.521	0.059700[a]
KDM5A	Lysine (K)-specific demethylase 5A	5927	hs|12p13.33	1.862	−1.000	0.074900[a]

GEO, Gene Expression Omnibus; miR, microRNA; OS, overall survival; RCC, renal cell carcinoma; TCGA, The Cancer Genome Atlas.

[aa]Poor prognosis in patients with low gene expression.

The TargetScan Human database showed that there is a binding site for *miR-101-5p* (positions 219-225) in the *DONSON* 3′-UTR (Figure 3D). A luciferase reporter assay was carried out using vectors containing these sequences to see if *miR-101-5p* directly regulates DONSON expression depending on the sequence. Cotransfection of *miR-101-5p* with vectors

FIGURE 4 *DONSON* knockdown assay by siRNA and the effect of cotransfection of *DONSON*/*miR-101-5p*. A, Cell proliferation activity after si-*DONSON* transfection into clear cell renal cell carcinoma ccRCC cells. B, Cell proliferation 72 h after reverse transfection with *miR-101-5p* and 48 h after forward transfection with the *DONSON* vector. C, Cell migration 48 h after reverse transfection with *miR-101-5p* and 24 h after forward transfection with the *DONSON* vector. D, Cell invasion 48 h after reverse transfection with *miR-101-5p* and 24 h after forward transfection with *DONSON* vector. E-G, Effects of si-*DONSON* on apoptosis, as assessed by apoptosis assays and western blot analysis of cleaved poly (ADP-ribose) polymerase (PARP), a marker of apoptosis. GAPDH was used as the loading control. Adriamycin (ADM) was used as a positive control. H, Effect of si-*DONSON* on the cell cycle. Flow cytometric analyses of cell-cycle-phase distributions in control cells and cells transfected with si-*DONSON*. Bar charts represent the percentages of si-*DONSON*-transfected cells relative to the control cells in the G_0/G_1, S, and G_2/M phases, respectively. **P* < .0001; ***P* < .005

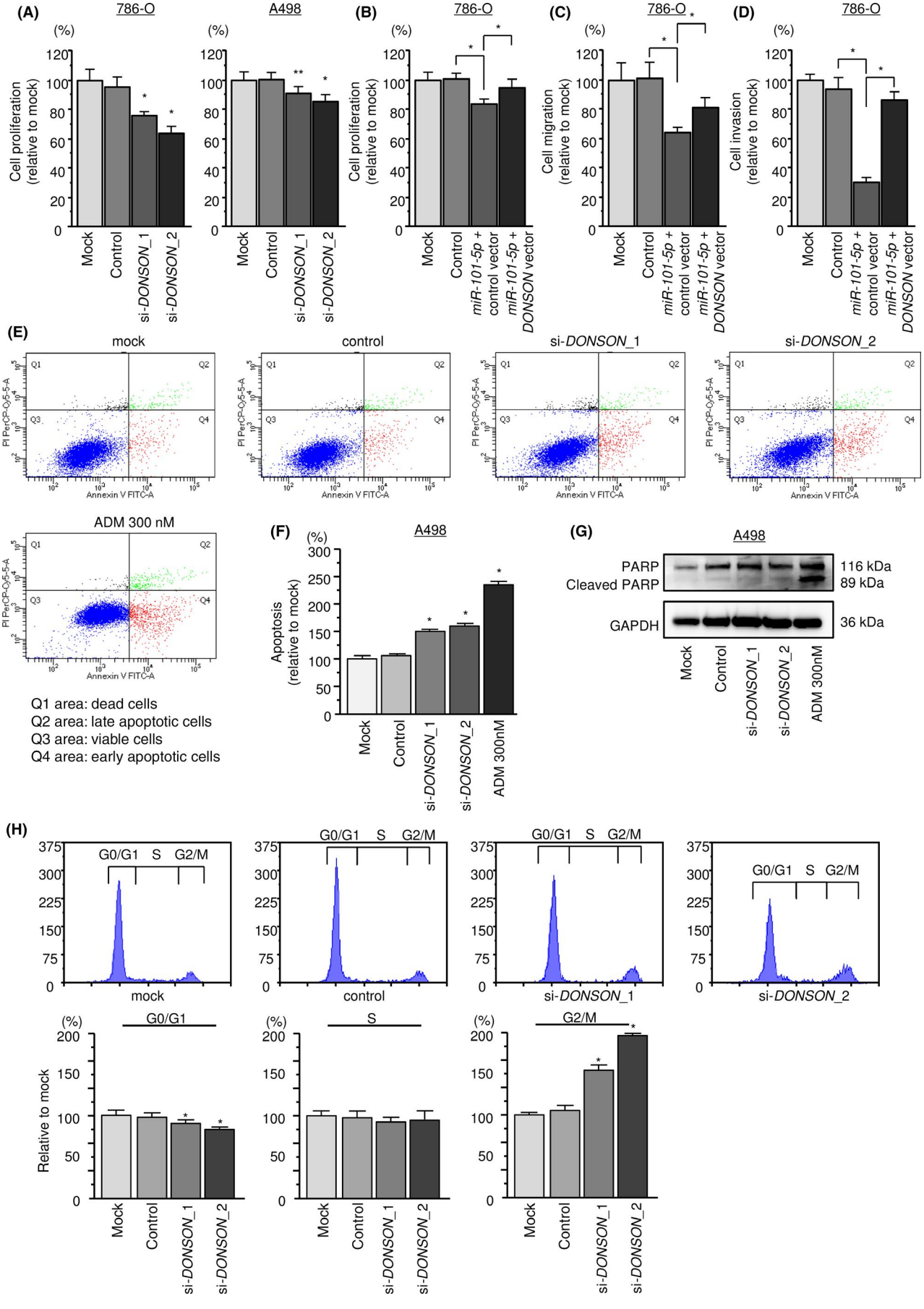
(A)
786-O
A498
(%)
Cell proliferation (relative to mock)
Mock
Control
si-DONSON_1
si-DONSON_2
(B)
786-O
Cell proliferation (relative to mock)
miR-101-5p + control vector
miR-101-5p + DONSON vector
(C)
786-O
Cell migration (relative to mock)
(D)
786-O
Cell invasion (relative to mock)
(E)
mock
control
si-DONSON_1
si-DONSON_2
ADM 300 nM
PI PerCP-Cy5-5-A
Annexin V FITC-A
Q1 area: dead cells
Q2 area: late apoptotic cells
Q3 area: viable cells
Q4 area: early apoptotic cells
(F)
A498
Apoptosis (relative to mock)
ADM 300nM
(G)
A498
PARP
Cleaved PARP
116 kDa
89 kDa
GAPDH
36 kDa
(H)
G0/G1 S G2/M
mock
control
si-DONSON_1
si-DONSON_2
Relative to mock

significantly suppressed luciferase activity compared to control cells (P = .0012) (Figure 3E).

3.6 | Clinical significance of *DONSON* expression in RCC patients

Conventional and propensity score-matched cohort analyses showed that patients with high *DONSON* expression showed poor prognosis (Figure 3F,G). The clinical background of the patients used for analysis is shown in Table S5. Furthermore, multivariate analysis has shown that gene expression is an independent prognostic factor (Figure 3H).

Combination analyses (*miR-101-5p* and *DONSON*) showed that patient group (low expression of *miR-101-5p* or high expression of *DONSON*) was a promising prognostic marker of patients with RCC (disease-free survival, P < .001; overall survival, P < .001) (Figure S5A,B). High expression of *DONSON* was involved in RCC pathogenesis, eg, tumor stage, metastasis, and grade (Figure S5C-G).

3.7 | Expression of DONSON in sunitinib-naïve and sunitinib-treated specimens

DONSON mRNA expression levels were significantly elevated in primary ccRCC tissues compared with those in adjacent noncancerous tissues (P = .0051) (Figure 3I). Furthermore, the expression levels in sunitinib-treated ccRCC tissues were highly expressed compared with those in primary ccRCC tissues (P < .0001) (Figure 3I).

In IHC staining, the expression of *DONSON* was gradually increased in the order of normal tissue, primary (sunitinib-naïve) RCC and sunitinib-treated ccRCC (Figure 3J-L).

3.8 | Knockdown assay and rescue study of DONSON in ccRCC cells

We confirmed that the expression levels of both *DONSON* mRNA and DONSON protein could be suppressed by si-*DONSON* transfection of ccRCC cells (Figure S6A,B). Downregulation of *DONSON* with siRNAs significantly attenuated cell proliferation (Figure 4A), migration and invasive potentials (Figure S6C,D).

In addition, introduction of both *DONSON* and *miR-101-5p* significantly restored cell proliferation, migration, and invasive activity, compared to cells transfected with *miR-101-5p* alone (Figure 4B-D). We confirmed that *DONSON* and *miR-101-5p* transfection restored DONSON protein expression (Figure S7).

Furthermore, the proportion of apoptotic cells was elevated in si-*DONSON*-transfected cells compared to control cells (Figure 4E,F). Transfection of si-*DONSON* did not apparently upregulate the level of cleaved PARP (Figure 4G). In cell cycle assays, the number of cells in the G_2/M phase were significantly elevated in si-*DONSON* transfected cells than control cells (Figure 4H).

3.9 | *DONSON* expression analyses combining clinical database and in vitro experiments

We identified differentially expressed genes that had similar expression behaviors to that of *DONSON* (Figure 5A). The GSEA showed that the top signaling pathway that was enriched in *DONSON* high RCC patients was the G_2/M checkpoint (Figure 5B). Furthermore, using the Kyoto Encyclopedia of Genes and Genomes pathways analysis, we found that the top significantly enriched pathway in 992 genes that had similar expression behavior to that of *DONSON* was DNA replication (Figure 5C,D). A heatmap visualization of gene expression of DNA replication pathway-related genes is shown in Figure 5E. Most of the genes coexpressed with *DONSON* were significantly associated with prognosis in ccRCC patients (Figure S8).

3.10 | Downstream genes mediated by *DONSON* in ccRCC cells

After microarray analysis, we identified 50 genes that were downregulated ($\log_2$ <−1.0) after transfection with si-*DONSON* (Table S6). *DONSON* expression was the most downregulated after si-*DONSON* transfection, indicating that these analyses were reliable and can be analyzed.

4 | DISCUSSION

A remarkable property of miRNA is that a single miRNA species can control a huge number of RNA transcripts under normal and pathologic conditions.[5] Therefore, miRNA-controlled intracellular RNA networks are being investigated in cancer cells. From RNA-seq-based miRNA signatures, some passenger strands of miRNAs, eg, *miR-144-5p*, *miR-455-5p*, and *miR-532-3p*, possess antitumor activity in ccRCC cells and their target genes contributed to its pathogenesis.[9,14,24] Passenger strands of miRNAs are generally not examined. Therefore, characterization of miRNA passenger strands in cancer regulatory networks is important for the development of novel diagnostic approaches.

In this study, we focused on *miR-101-5p* (the passenger strand of pre-*miR-101*) and investigated the associated regulatory RNA networks in ccRCC cells. Previous studies of *miR-101-3p* (the guide strand of pre-*miR-101*) found that it was often downregulated in a wide range of human cancers and acted as an antitumor miRNA through its targeting of several oncogenes.[17] Our miRNA signature of patients with sunitinib failure showed that *miR-101-5p* was the most downregulated miRNA in cancer tissues. Moreover, ectopic expression of miR-101-3p significantly blocked the aggressive phenotype.[8] Direct control of enhancer of zeste homolog 2 (*EZH2*), which functions as an oncogene in various cancers, has been proven in many studies.[25] Our previous study showed that antitumor *miR-101-3p* directly regulated ubiquitin like with phd and ring finger domains 1 (*UHRF1*) in ccRCC cells.[8] Aberrant expression of *UHRF1* was observed in several cancers and its overexpression facilitated cancer

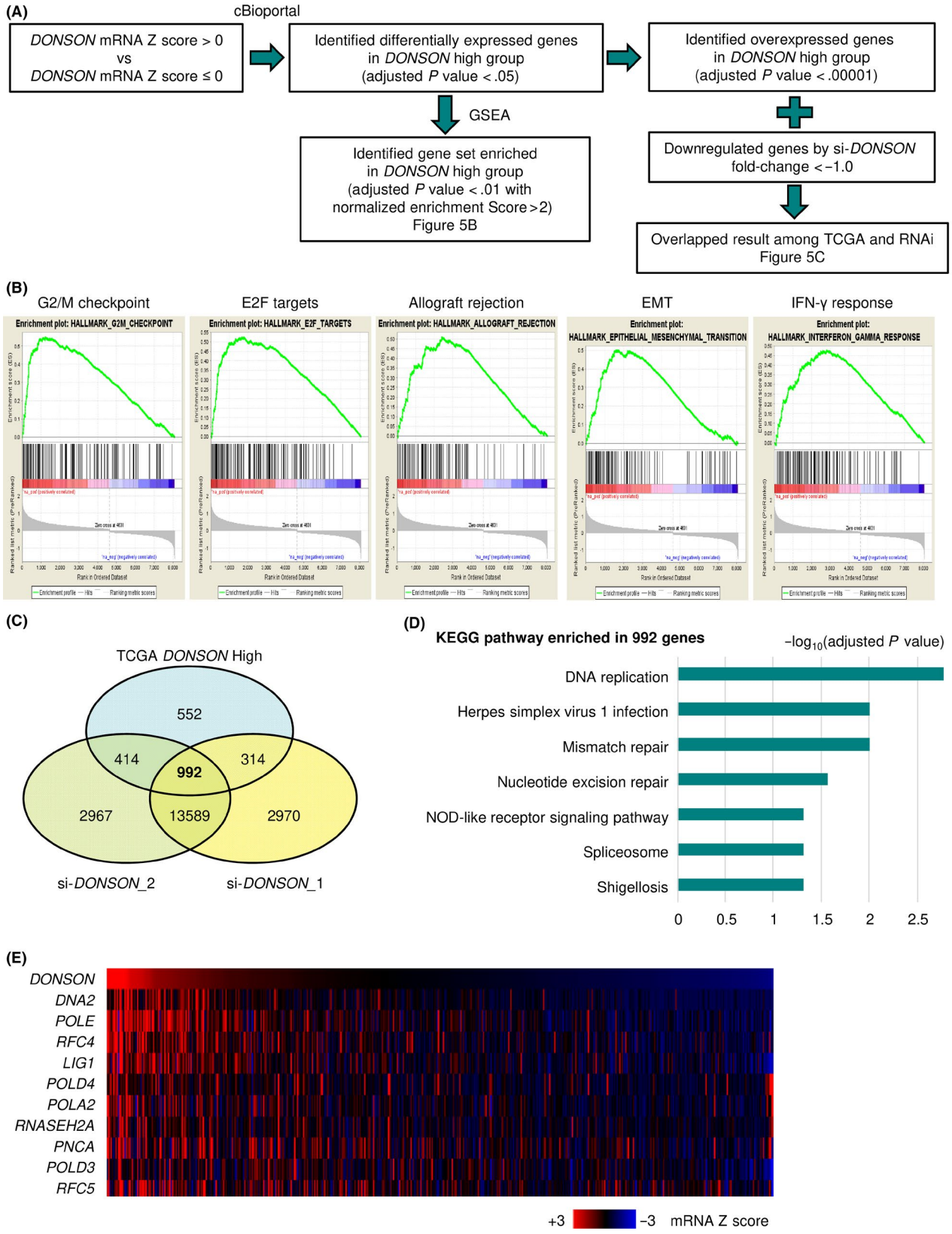

FIGURE 5 The Cancer Genome Atlas (TCGA) database analysis of clinical significance and function of *DONSON* in clear cell renal cell carcinoma. A, Identification of differentially expressed genes in the *DONSON* high group and the si-*DONSON* group. B, Gene Set Enrichment Analysis (GSEA) of mRNA expression levels of *DONSON* high RCC patients. C, Venn diagram showed the overlapped 992 genes among TCGA and RNAi. D, Significantly enriched pathways including 992 genes that showed similar expression behaviors with *DONSON* using Kyoto Encyclopedia of Genes and Genomes (KEGG) pathways analysis. E, Heatmap visualization of gene expression of DNA replication pathway-related genes

cell malignancy.[26] In contrast to those studies of *miR-101-3p*, investigation of *miR-101-5p* has rarely been undertaken.

In a few reports, *miR-101-5p* expression was found to be downregulated. *miR-101-5p* was shown to inhibit cell aggressiveness through targeting of C-X-C motif chemokine ligand 6 (*CXCL6*) in cervical cancer and nonsmall-cell lung carcinoma.[27,28] To our knowledge, the present study is the first report to show the antitumor functions of *miR-101-5p* in ccRCC. The elucidation of *miR-101-5p*-controlled novel oncogenic networks in ccRCC cells is particularly important.

In further analysis of *miR-101-5p* in ccRCC, we identified candidate target oncogenes using genome-wide expression analysis. A total of 38 oncogenes was found to be regulated by *miR-101-5p*. Of these oncogenic targets, the high expression of 13 genes was a significant prognostic factor for ccRCC. We focused on *DONSON* because it was directly regulated by *miR-101-5p* and it was the best predictor of poor prognosis of patients. Recently, *DONSON* was found to encode a novel fork protein factor and play an important role in mammalian DNA replication and genome stability. Moreover, its mutation caused microcephalic dwarfism.[29-33] Previous studies showed that DONSON is a member of replisome complex and protected stalled or damaged replication forks. Also, DONSON interacted with several DNA replication factors and facilitated the activation of the intra-S-phase and G_2/M cell cycle checkpoints.[29] Minichromosome maintenance (*MCM*) proteins are crucial DNA replication genes that interact with DONSON. They are often overexpressed in ccRCC tissues and could be useful prognostic markers in ccRCC patients.[34,35] Aberrant expression of DONSON was observed in sunitinib-treated ccRCC and silencing *DONSON* inhibited cell growth and induced apoptosis and cell cycle arrest in G_2/M phase. Our GSEA data analysis revealed that the EMT pathway was significantly enriched in the DONSON high expression group. Previous reports showed that EMT-associated genes were overrepresented in TKI-resistant ccRCC tissues compared with pretreatment ccRCC tissues.[36] Tyrosine kinase inhibitor-resistant RCC cells promoted the activities of EMT-related genes, indicating that EMT was involved in the mechanism of resistance to TKI.[36] These findings might explain the aberrant expression of DONSON that was detected in sunitinib-treated ccRCC tissues. Also, our data showed that *miR-101-5p* regulated the expression of several EMT-related genes, indicating *miR-101-5p* might have a relation to resistance to TKI treatment.

Expression of *DONSON* was an independent strong prognostic marker (better than tumor stage or pathological grade) and was associated with ccRCC patient survival in a propensity score-matched cohort. Aberrant expression of *DONSON* has serious effects on the prognosis of patients with ccRCC. However, elucidation of the molecular mechanism for controlling *DONSON* expression in ccRCC cells is not sufficient. Exploring the causes of overexpression of *DONSON* in ccRCC cells is an important issue. Recent studies showed that expression of circular RNAs in cancer cells have participated in oncogenesis.[37,38] Interestingly, overexpression of circ-*DONSON* (derived from exon 3 to exon 8 of *DONSON* mRNA) was detected in gastric cancer and its aberrant expression promoted gastric cancer cell aggressiveness through initiated *SOX4* expression.[31] The oncogenic roles of the circ-*DONSON* in ccRCC cells need to be investigated in the future.

We searched genes/pathways in ccRCC cells that were mediated by *DONSON*. Interestingly, DNA replication, mismatch repair, nucleotide excision repair, and spliceosome pathways were identified as *miR-101-5p* regulatory pathways. Among these pathways, genes involved in the DNA replication pathway (*DNA2*, *POLE*, *REFC4*, *LIG1*, *POLD4*, *POLA2*, and *RNASEH2A*) predicted poor prognosis of ccRCC patients. The replisome is a complex molecular machine that comprises the DNA replication apparatus.[39] The replisome unwinds double-stranded DNA into single strands.[40] These findings suggest that aberrantly expressed genes involved in the replisome affected ccRCC pathogenesis.

In conclusion, this is the first research to report that *miR-101-5p* acted as an antitumor miRNA in ccRCC cells. Several oncogenic targets regulated by *miR-101-5p* were closely involved with ccRCC pathogenesis. Moreover, we found that *DONSON* and replisome genes, which we identified from analyses of genes controlled by antitumor *miR-101-5p*, could be novel prognostic and therapeutic targets in ccRCC.

ACKNOWLEDGMENTS

The present study was supported by KAKENHI grants 16H05462, 17K11160, 18K09338, 18K16685, 18K16723, and 18K16724.

CONFLICT OF INTEREST

The authors declare no conflict of interest. NN is an employee of MSD K.K., a subsidiary of Merck & Co., Inc and reports personal fees from MSD K.K. outside this study.

ORCID

Yasutaka Yamada https://orcid.org/0000-0002-0070-1590
Nijiro Nohata https://orcid.org/0000-0002-6816-2984
Takayuki Arai https://orcid.org/0000-0002-3888-9576

REFERENCES

1. Capitanio U, Montorsi F. Renal cancer. *Lancet*. 2016;387(10021):894-906.
2. Pierorazio PM, Johnson MH, Patel HD, et al. Management of renal masses and localized renal cancer: systematic review and meta-analysis. *J Urol*. 2016;196(4):989-999.
3. Cairns P. Renal cell carcinoma. *Cancer Biomarkers*. 2010;9(1–6):461-473.
4. Cohen HT, McGovern FJ. Renal-cell carcinoma. *N Engl J Med*. 2005;353(23):2477-2490.
5. Bartel DP. MicroRNAs: genomics, biogenesis, mechanism, and function. *Cell*. 2004;116(2):281-297.
6. Goto Y, Kurozumi A, Enokida H, Ichikawa T, Seki N. Functional significance of aberrantly expressed microRNAs in prostate cancer. *Int J Urol*. 2015;22(3):242-252.
7. Adams BD, Kasinski AL, Slack FJ. Aberrant regulation and function of microRNAs in cancer. *Curr Biol*. 2014;24(16):R762-R776.
8. Goto Y, Kurozumi A, Nohata N, et al. The microRNA signature of patients with sunitinib failure: regulation of UHRF1 pathways by microRNA-101 in renal cell carcinoma. *Oncotarget*. 2016;7(37):59070-59086.
9. Yamada Y, Arai T, Kojima S, et al. Anti-tumor roles of both strands of the miR-455 duplex: their targets SKA1 and SKA3 are involved in the pathogenesis of renal cell carcinoma. *Oncotarget*. 2018;9(42):26638-26658.

10. Yamada Y, Sugawara S, Arai T, et al. Molecular pathogenesis of renal cell carcinoma: Impact of the anti-tumor miR-29 family on gene regulation. *Int J Urol*. 2018;25(11):953-965.
11. Goto Y, Kurozumi A, Arai T, et al. Impact of novel miR-145-3p regulatory networks on survival in patients with castration-resistant prostate cancer. *Br J Cancer*. 2017;117(3):409-420.
12. Koshizuka K, Nohata N, Hanazawa T, et al. Deep sequencing-based microRNA expression signatures in head and neck squamous cell carcinoma: dual strands of pre-miR-150 as antitumor miRNAs. *Oncotarget*. 2017;8(18):30288-30304.
13. Arai T, Kojima S, Yamada Y, et al. Pirin: a potential novel therapeutic target for castration-resistant prostate cancer regulated by miR-455-5p. *Mol Oncol*. 2019;13(2):322-337.
14. Yamada Y, Arai T, Kojima S, et al. Regulation of antitumor miR-144-5p targets oncogenes: direct regulation of syndecan-3 and its clinical significance. *Cancer Sci*. 2018;109(9):2919-2936.
15. Yamada Y, Koshizuka K, Hanazawa T, et al. Passenger strand of miR-145-3p acts as a tumor-suppressor by targeting MYO1B in head and neck squamous cell carcinoma. *Int J Oncol*. 2018;52(1):166-178.
16. Mah SM, Buske C, Humphries RK, Kuchenbauer F. miRNA*: a passenger stranded in RNA-induced silencing complex? *Crit Rev Eukaryot Gene Expr*. 2010;20(2):141-148.
17. Wang CZ, Deng F, Li H, et al. MiR-101: a potential therapeutic target of cancers. *Am J Transl Res*. 2018;10(11):3310-3321.
18. Yamada Y, Arai T, Sugawara S, et al. Impact of novel oncogenic pathways regulated by antitumor miR-451a in renal cell carcinoma. *Cancer Sci*. 2018;109(4):1239-1253.
19. Goto Y, Kojima S, Kurozumi A, et al. Regulation of E3 ubiquitin ligase-1 (WWP1) by microRNA-452 inhibits cancer cell migration and invasion in prostate cancer. *Br J Cancer*. 2016;114(10):1135-1144.
20. Goto Y, Kojima S, Nishikawa R, et al. MicroRNA expression signature of castration-resistant prostate cancer: the microRNA-221/222 cluster functions as a tumour suppressor and disease progression marker. *Br J Cancer*. 2015;113(7):1055-1065.
21. J A. . OncoLnc: linking TCGA survival data to mRNAs, miRNAs, and lncRNAs. PeerJ computer. *Science*. 2016;2:e67.
22. Gao J, Aksoy BA, Dogrusoz U, et al. Integrative analysis of complex cancer genomics and clinical profiles using the cBioPortal. *Sci Signal*. 6(269):pl1-pl1.
23. Cerami E, Gao J, Dogrusoz U, et al. The cBio cancer genomics portal: an open platform for exploring multidimensional cancer genomics data. *Cancer Discov*. 2012;2(5):401-404.
24. Yamada Y, Arai T, Kato M, et al. Role of pre-miR-532 (miR-532-5p and miR-532-3p) in regulation of gene expression and molecular pathogenesis in renal cell carcinoma. *Am J Clin Exp Urol*. 2019;7(1):11-30.
25. Kim KH, Roberts CW. Targeting EZH2 in cancer. *Nat Med*. 2016;22(2):128-134.
26. Sidhu H, Capalash N. UHRF1: The key regulator of epigenetics and molecular target for cancer therapeutics. *Tumour Biol*. 2017;39(2):1010428317692205.
27. Chen Q, Liu D, Hu Z, Luo C, Zheng SL. miRNA-101-5p inhibits the growth and aggressiveness of NSCLC cells through targeting CXCL6. *Onco Targets Ther*. 2019;12:835-848.
28. Shen W, Xie XY, Liu MR, Wang LL. MicroRNA-101-5p inhibits the growth and metastasis of cervical cancer cell by inhibiting CXCL6. *Eur Rev Med Pharmacol Sci*. 2019;23(5):1957-1968.
29. Reynolds JJ, Bicknell LS, Carroll P, et al. Mutations in DONSON disrupt replication fork stability and cause microcephalic dwarfism. *Nat Genet*. 2017;49(4):537-549.
30. Nordquist SK, Smith SR, Pierce JT. Systematic functional characterization of human 21st chromosome orthologs in *Caenorhabditis elegans*. *G3*. 2018;8(3):967-979.
31. Ding L, Zhao Y, Dang S, et al. Circular RNA circ-DONSON facilitates gastric cancer growth and invasion via NURF complex dependent activation of transcription factor SOX4. *Mol Cancer*. 2019;18(1):45.
32. Evrony GD, Cordero DR, Shen J, et al. Integrated genome and transcriptome sequencing identifies a noncoding mutation in the genome replication factor DONSON as the cause of microcephaly-micromelia syndrome. *Genome Res*. 2017;27(8):1323-1335.
33. Schulz S, Mensah MA, de Vries H, et al. Microcephaly, short stature, and limb abnormality disorder due to novel autosomal biallelic DONSON mutations in two German siblings. *Eur J Hum Genet*. 2018;26(9):1282-1287.
34. Zhong H, Chen B, Neves H, et al. Expression of minichromosome maintenance genes in renal cell carcinoma. *Cancer Manag Res*. 2017;9:637-647.
35. Fei L, Xu H. Role of MCM2-7 protein phosphorylation in human cancer cells. *Cell Biosci*. 2018;8:43.
36. Hwang HS, Go H, Park JM, et al. Epithelial-mesenchymal transition as a mechanism of resistance to tyrosine kinase inhibitors in clear cell renal cell carcinoma. *Lab Invest*. 2019;99(5):659-670.
37. Meng S, Zhou H, Feng Z, et al. CircRNA: functions and properties of a novel potential biomarker for cancer. *Mol Cancer*. 2017;16(1):94.
38. Kristensen LS, Hansen TB, Veno MT, Kjems J. Circular RNAs in cancer: opportunities and challenges in the field. *Oncogene*. 2018;37(5):555-565.
39. Gao Y, Cui Y, Fox T, et al. Structures and operating principles of the replisome. *Science*. 2019;363(6429):eaav7003.
40. Burnham DR, Kose HB, Hoyle RB, Yardimci H. The mechanism of DNA unwinding by the eukaryotic replicative helicase. *Nat Commun*. 2019;10(1):2159.

SUPPORTING INFORMATION

Additional supporting information may be found online in the Supporting Information section.

How to cite this article: Yamada Y, Nohata N, Uchida A, et al. Replisome genes regulation by antitumor *miR-101-5p* in clear cell renal cell carcinoma. *Cancer Sci*. 2020;111:1392–1406. https://doi.org/10.1111/cas.14327